Determination of the Lawson Number (Fusion Triple Product) for Projectile-Driven ICF from Simulation Output

D. A. Chapman, M. R. Betney and N. A. Hawker
First Light Fusion Ltd., Unit 10 Oxford Industrial Park, Yarnton, OX5 1QU, United Kingdom
(Dated: April 4, 2022)

A simple, generalised methodology is developed for the estimation of the Lawson number (a.k.a. the 'fusion triple product') and related quantities of interest, using information contained in the diagnostic probe files produced by First Light Fusion's (FLF) Hytrac and B2 design codes. The calculation of the confinement time considers cases where the neutron output of the target comes in a number of distinct 'emission events', each of which may be multi-modal in nature and separated from one another in time over the target operation. For targets whose yield comes from a single pulse of neutrons, our modified definition reduces to the commonly used definition for conventional laser-driven hot spot ignition designs. The number density and temperature of the fuel ions are based on a weighted average of suitable characteristic values from all neutron emission events that depend on the reaction rate in the fusion fuel. The fuel ion density is also generalised to account for arbitrary mixtures of reactive and inert ion species. Three examples are given, showing detailed traces and the operation of the method. The tool has then been run on a large number of FLF designs, including future pipeline designs and the design which has recently demonstrated fusion [1, 2]. The results are plotted following Wurzel and Hsu [3] and reveal the unique nature of FLF's approach, which has very high values of the product of fuel ion number density and confinement time.

Keywords: Lawson number, fusion triple product, Wurzel and Hsu, Fusion Energy Base, confinement time, burn-weighted average, BWA, fusion performance average, FPA

I. INTRODUCTION

The motivation of the present work is to provide the ability to quantitatively compare the predicted fusion performance of FLF's target designs with the many and various existing fusion schemes. Furthermore, being able to quantify the fusion performance of systems without directly referring to neutron yields is extremely useful from the perspective of optimisation work for future target design and development, as well as for tracking the historical progress of the company's technical capabilities. Given the extremely diverse nature of the present global effort towards achieving controlled fusion, such comparisons require careful consideration and an open, collaborative conversation across the many facets of the industry. To this end, Wurzel and Hsu [3] have recently published a landmark paper which seeks to undertake just such a broad review and present a quantitative and unbiased comparison. Note that at the time of writing Wurzel and Hsu's paper is a pre-print available on the arXiv server, although the authors anticipate publication in Q2 of 2022. Their work is drawn from an online database curated by Wurzel: `www.fusionenergybase.com`, from which all the data described in this report has been taken.

As discussed in Ref. [3], the principal figure of merit through which the performance of fusion systems may be judged is the well-known 'fusion triple product', often also referred to as the 'Lawson number', originally introduced by J. D. Lawson in a declassified technical report from 1955 (later published as Ref. [4]) and subsequently expanded on in numerous works over several decades (see the numerous references cited in Ref. [3]).

The Lawson number/FTP is written in its most general form as the product of the number density, n_i, and temperature, T_i, of fuel ions in a fusing plasma and a meaningful time scale, τ, over which the fusion occurs:

$$L = n_i T_i \tau \,. \tag{1}$$

The interpretation of Eq. (1) is most commonly understood to mean the density and temperature of the fuel during fusion and, in particular, the time scale is associated with a 'confinement time' for the assembled thermonuclear fuel. A detailed discussion on the origin of the expression and the nuances that must be considered in the context of real fusion systems is covered admirably in Ref. [3], and will not be repeated here.

The most important differences that are relevant to the current discussion are that the various terms in Eq. (1) follow different prescriptions for the main two families of devices used in controlled fusion research; magnetic confinement fusion (MCF) and inertial confinement fusion (ICF). These are:

MCF (mostly tokamak-like devices):

Here, Eq. (1) is to be interpreted as the triple product

$$L\ [\mathrm{keV\,s/m^3}] = n_{i0}\ [1/\mathrm{m^3}] \times T_{i0}\ [\mathrm{keV}] \times \tau_E^*\ [\mathrm{s}]\,, \tag{2}$$

in which the following parameters have been defined:

- n_{i0}: the density of fuel ions (typically always deuterons and tritons) in the centre of a cross sectional slice of the plasma profile. This may be measured using well-founded diagnostic techniques for tenuous plasmas.

- T_{i0}: as above, but for the fuel ion temperature.
- τ_E^*: the 'modified' energy confinement time, which accounts for thermal conduction losses and fusion product heating from the idealised system, as well as the transient start-up period where a potentially significant fraction of the energy consumed goes into heating the fuel to its operating conditions.

ICF (mostly laser-driven systems):

For laser-driven ICF, the Lawson number can either be assessed using the relationship

$$\begin{aligned} L\ [\mathrm{keV\,s/m^3}] &= 2.533\times10^{21}\times \mathrm{YOC}^{\,\mu} \\ &\quad\times\left[(\rho R)^{\mathrm{no}\ \alpha}_{\mathrm{tot(n)}}\ [\mathrm{g\,cm^{-2}}]\times\langle T_i\rangle^{\mathrm{no}\ \alpha}_{\mathrm{n}}\ [\mathrm{keV}]\right]^{0.8} \\ &\equiv n_i\tau\ [\mathrm{s/m^3}]\times\langle T_i\rangle_{\mathrm{n}}\ [\mathrm{keV}]\,, \end{aligned} \tag{3}$$

due to Betti et al. [5], in which $\mu = 0.4-0.5$, or through the simple relationship to the pressure and time scale related to the stagnation of the implosion over which the fusion burn occurs

$$L\ [\mathrm{keV\,s/m^3}] = 1.04\times10^{20}\times p_{\mathrm{stag}}\ [\mathrm{Gbar}]\times\tau_{\mathrm{stag}}\ [\mathrm{ns}]\,, \tag{4}$$

as favoured by Christopherson et al. [6]. In the foregoing expressions (3) and (4) the following parameters have been defined:

- $(\rho R)^{\mathrm{no}\ \alpha}_{\mathrm{tot(n)}}$: the total areal density of the compressed target in the absence of heating due to stopping of α particles.
- $\langle T_i\rangle_{\mathrm{n}}$, $\langle T_i\rangle^{\mathrm{no}\ \alpha}_{\mathrm{n}}$: the 'neutron-averaged' ion temperature, with/without α-heating.
- YOC: the 'yield over clean', being either the ratio of measured to simulated neutron yield or, less commonly, the ratio of predicted yields obtained from 3D to 2D simulations.
- $n_i\tau$: the Lawson n-τ (double product) parameter, defined explicitly through the relationship encapsulated in Eq. (3).
- p_{stag}: the average total plasma pressure in the fusion fuel achieved during the stagnation phase of the implosion. This usually inferred from post-shot tuned simulations using measurements of 'bang time' and incident shock speed.
- τ_{stag}: the duration of the stagnation phase, which is defined as the full-width at half-maximum (FWHM) of the temporal profile of the total neutron production rate of the target [6].

For the sake of further clarification, it should be noted that the determination of $(\rho R)^{\mathrm{no}\ \alpha}_{\mathrm{tot(n)}}$ and $\langle T_i\rangle^{\mathrm{no}\ \alpha}_{\mathrm{n}}$ can only be made using simulations for the obvious reason that one cannot 'turn off' the fusion product heating. In contrast, the true neutron-averaged ion temperature $\langle T_i\rangle_{\mathrm{n}}$ may be determined from either simulations or experimental diagnostics. Furthermore, the usage of Eq. (4) as an alternative definition of the Lawson number is not general since the equivalence $\frac{1}{2}p_{\mathrm{stag}} \propto n_iT_i$ only holds for fusion fuels composed purely of hydrogen isotopes, such as pure deuterium of a deuterium-tritium mixture, under ideal (non-degenerate and weakly coupled) conditions. If the fuel features elements other than hydrogen, e.g. due to mix, one may generalise the relationship to $p_i = p_{\mathrm{stag}}/(1+\langle Z_i\rangle) \propto n_iT_i$. This is further complicated if the fuel contains one (or more) populations of inert ion species. In the most general case, where the mixture is fully arbitrary and the conditions are non-ideal, a simple relationship may not exist at all due to the non-linearity of the equation of state. It is therefore preferable to consider the product of the simulated/measured number density and temperature of the fuel ions, rather than the stagnation pressure. More discussion will be given to this point later on.

As stated, the aim of this letter is to provide a reasonable estimate for the Lawson number (and related parameters) to capture the progression and indicative performance of FLF's target designs; both historical and recent. Of course, the most credible manner in which to pursue this goal would be to measure experimentally the relevant parameters in order to follow the well-defined methodologies described above for laser-driven ICF (the fusion scheme to which FLF's approach is most aligned). In the absence of such data, however, one must rely solely on simulations to provide the relevant estimates. Since it is generally intractable to base any methodology on requiring the full spatial and temporal output from simulations, i.e., requiring the plasma conditions from the entire multi-dimensional grid at all time steps, we consider instead using only the time-dependent outputs produced by the various in-built probes available in FLF's codes: Hytrac and B2. The second important consideration that is addressed is the generalisation of the loose criteria that form the 'standard' approach discussed by Wurzel and Hsu. In this regard, the meaning and evaluation of the confinement time is extended to targets in which multiple neutron emission events are induced due to the more complex hydrodynamics associated with the implosion of FLF's targets.

II. METHODOLOGY

In order to remain as closely aligned as possible to the accepted definitions of the Lawson number discussed in the previous section, we consider a true triple product composed of independent assessments of the number density and temperature of the fuel ions and the confinement time. Thus, the aim is to assess the viability of using the information available in the Hytrac/B2 probe outputs to approximate the desired quantities.

A. Confinement time

As will become clear, the most important aspect of the methodology developed in this work is the estimation of the confinement time. Christopherson et al. [6] have investigated the approximate scaling of ignition criteria for hot spot-style ICF using integrated simulations, leading to an approximate relationship between the stagnation time, $\tau_{\rm stag}$, and the system's confinement time as $\tau \approx \frac{1}{3}\tau_{\rm stag}$. Note that Wurzel and Hsu specifically denote the stagnation time as '*the full-width half-maximum (FWHM) of the neutron-emission history*' [3]. The factor of 1/3 is the result of three considerations related to the production and transport of the fusion products (α particles) throughout the burn phase (see Ref. [6] for more details). Given that the Lawson number is an inherently approximate figure of merit, we choose to ignore this factor as it is not clear how to construct suitable analogues for FLF's targets.

A much larger difference to the standard methodology for laser-driven ICF that must be considered arises due to the complexity of the different target geometries studied at FLF. Even factoring in real 3D effects, it is expected that the neutron emission in hot spot ignition designs should occur in a single, strong pulse, produced during the stagnation of the main fuel assembly. For many of the targets of interest to FLF the neutron output comes instead from a succession of neutron production pulses, all originating from a single global implosion of a single volume of fuel, the character and temporal separation of which often vary widely over the design space. For the present application it is therefore desirable to generalise the definition of confinement (stagnation) time to an arbitrary number of neutron 'emission events'. Naturally, it is important that this generalised definition should reduce to the single-pulse (hot spot design) case, i.e., for a single neutron emission event: $\tau \propto \mathrm{FWHM}(\partial Y/\partial t)$.

To fulfill the foregoing restriction, we choose to base our approach solely on the total neutron production rate history captured in the probe files produced by Hytrac/B2, and consider a total confinement time given by the sum over all distinct neutron emission events

$$\tau \approx \sum_{\rm events} \tau_{\rm event} = \sum_{\rm events} \mathrm{FWHM}\left(\frac{\partial Y}{\partial t}\right)_{\rm event} . \quad (5)$$

The identification and characterisation (in terms of their FWHM values) of all the relevant peaks in the total neutron production rate history thus constitutes the core of our estimation for τ.

1. *Identifying relevant peaks in the neutron production history*

Determining whether or not a particular peak is 'relevant' can be formalised using a descending integration method (DIM). In the context of the current problem, consider the normalised total neutron production rate

$$R(t) = \frac{\partial Y/\partial t}{\max(\partial Y/\partial t)} , \quad (6)$$

where $\max(\partial Y/\partial t)$ denotes the global maximum rate, i.e., the largest value of $\partial Y/\partial t$ for all times $0 \le t \le t_{\rm end}$. The normalised rate $R(t)$ can be thresholded by subtracting a constant value, $1 - R_0$ with $R_0 < 1$, and retaining only positive values:

$$R'(t; R_0) = \max[0, R(t) - (1 - R_0)] . \quad (7)$$

The effective neutron yield calculated by integrating the thresholded normalised rate with respect to time is then

$$Y_{\rm eff}(R_0) = \max\left(\frac{\partial Y}{\partial t}\right) \int_0^{t_{\rm end}} \mathrm{d}t\, R'(t; R_0) . \quad (8)$$

The object of the DIM is then to iteratively increase the value of R_0 asymptotically to unity and evaluating Eq. (8) until the condition

$$Y_{\rm eff}(R_0) = f Y_{\rm tot} = f \int_0^{t_{\rm end}} \mathrm{d}t\, \frac{\partial Y(t)}{\partial t} \quad (9)$$

is satisfied for some pre-defined fraction of the total neutron yield, f. By default the latter is set to $f = 0.99$, although it is a free parameter in the model. The DIM procedure therefore returns the indices of the array of values for $\partial Y/\partial t$ containing features which cumulatively contain the desired fraction of the total yield from the simulation.

As shown in Fig. 1, as $f \to 1$ we find a progressive decrease in the value of the threshold R_0 (black horizontal thin dashed lines on each panel), which identifies different sub-regions of the full total neutron production rate history (thick black dashed curve). Each sub-region is emphasised by the differently coloured thick curves that are separated by regions containing normalised rates below the threshold. Note that as the fraction is increased some sub-regions join together, with new sub-regions corresponding to shallow peaks emerging. For the example shown, the main structure eventually merges for $f = 0.99$ into a single set of structures (blue curve), with a small additional peak at late time emerging (very small orange curve at 1780.8 ns).

2. *Finding the locations of peaks within a sub-region*

With the indices delineating the different sub-regions determined, the next step is to identify the times of the various peaks (labelled j) contained in each one. This is achieved by progressively solving for the roots of the derivative of the curves in each sub-region, i.e., finding all values of $t^j_{\rm peak}$, such that

$$\frac{\partial R(t^j_{\rm peak})}{\partial t} = 0 \quad (10)$$

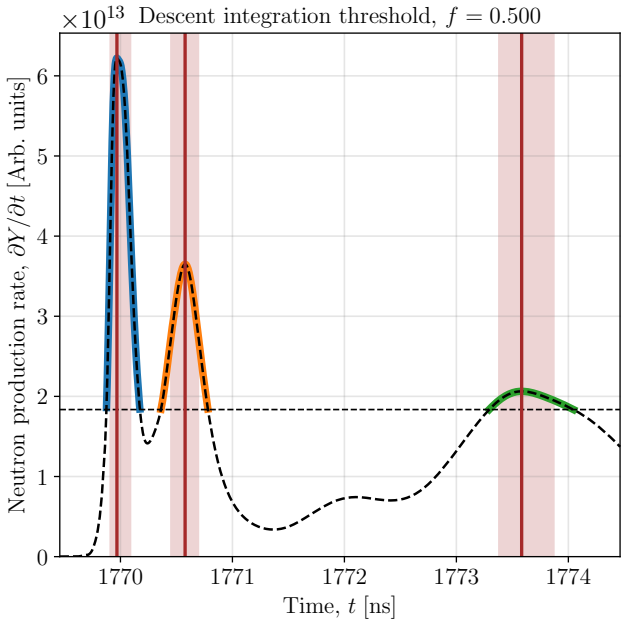

(a) Three sub-regions of interest are identified for $f = 0.5$.

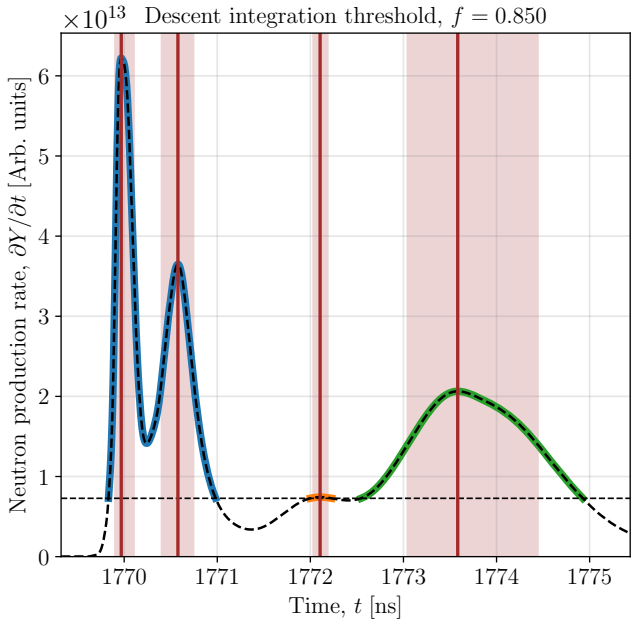

(b) Three different sub-regions are found for $f = 0.85$.

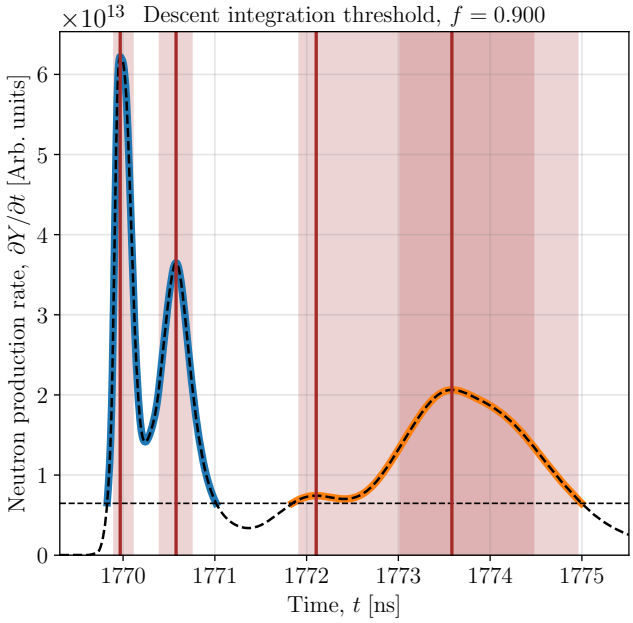

(c) The two later-time sub-regions merge for $f = 0.9$.

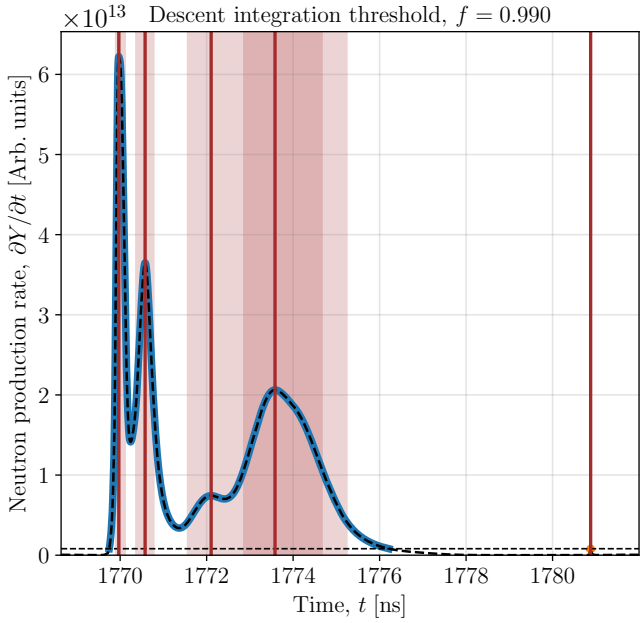

(d) All previous sub-regions merge for $f = 0.99$, with a very small new late-time sub-region identified for $f = 0.99$.

Figure 1. **Influence of the fraction f on the identification of distinct peak structures via the DIM method**: For $f = 0.5$ (a), three distinct structures are identified (blue, orange and green thick curves). The first two peaks from Panel (a) merge and a new intermediate peak emerges when $f = 0.85$ (b). Increasing to $f = 0.9$ (c) enables the two later peaks from Panel (b) to merge, leaving only two distinct features. When the fraction is increased to $f = 0.99$ (d) the two sub-regions from Panel (c) merge and a new, nearly invisible sub-region containing an essentially negligible peak emerges at $t \approx 1780.8$ ns. In each panel, the vertical brown lines indicate the locations of the individual peaks, and the shaded regions surrounding them are within their full-width at half-maximum (FWHM) regions. Note that some of the FWHM boundaries of different peaks may overlap either partially or fully (the *peak-in-a-peak* scenario).

and simultaneously

$$\frac{\partial R(t^j_{\rm peak}-\Delta t^j_-)}{\partial t}>0\,,\quad \frac{\partial R(t^j_{\rm peak}+\Delta t^j_+)}{\partial t}<0\,. \quad (11)$$

Here, $\Delta t^j_\pm$ is the time difference computed from the data about $t=t^j_{\rm peak}$. Note that in order to remove the undue influence of fast-varying noise in the total neutron production rate the peaks are located after the data has been smoothed using a Savitzky-Golay filter [7]. This procedure results in the values of $t_{\rm peak}$ shown by brown vertical thin lines in each panel of Fig. 1.

3. Determination of the FWHM of a particular peak

The FWHM of peak j in the total neutron production rate is defined as the difference of two 'boundary' times

$$\text{FWHM}(\partial Y/\partial t)^j_{\rm peak}=t^j_{+1/2}-t^j_{-1/2}\,. \quad (12)$$

As will be shown later, it will prove important to distinguish between these two boundary times, and to do so we refer to $t^j_{-1/2}$ as the 'early' boundary time of peak j, and to $t^j_{+1/2}$ as the 'late' boundary time of peak j. The boundary times themselves are defined via the implicit relationship

$$R(t^j_{\pm 1/2})=\frac{1}{2}\Big(R(t^j_{\rm peak})+R_0\Big)\,. \quad (13)$$

To calculate the boundary times we use a straightforward algorithm which decrements/increments (reverse/-forward search) the element index of the normalised rate, starting at the peak time in each case, until the condition $R(t_i)\leq\frac{1}{2}(R(t^j_{\rm peak})+R_0)$ is fulfilled. In both cases, this returns the first element index with a normalised rate $R\leq 1/2$, which is denoted i. The first element with a normalised rate $R>1/2$ is then $i+1$ for the early boundary time and $i-1$ for the late boundary time. With these indices determined, the boundary times are subsequently refined using linear interpolation. The specific expressions are:

$$t^j_{-1/2}=t_i+\frac{1/2-R(t_i)}{R(t_{i+1})-R(t_i)}(t_{i+1}-t_i)\,, \quad (14)$$

and

$$t^j_{+1/2}=t_{i-1}+\frac{1/2-R(t_{i-1})}{R(t_i)-R(t_{i-1})}(t_i-t_{i-1})\,. \quad (15)$$

4. Refining FWHM boundary times for partially/fully overlapping peaks

So far, we have described an idealised situation in which one may confidently apply the foregoing algorithm to a sub-region containing either a single peak or a series of *clearly differentiated* peaks. One may then identify each distinct peak with a neutron emission event and use Eq. (5) to compute the total confinement time of the system. However, it is relatively common to find that the total neutron production rate in a sub-region describes a complex structure with numerous peaks (see Fig. 1), some of which are not only not clearly differentiated but are fully subsumed within one another. To formalise what we mean by 'clearly differentiated peaks' consider the cartoon shown in Fig. 2. In this example, the development of a single peak into two peaks is shown, with each progression gradually reducing the amplitude of the inter-peak valley. The structures shown in Panels (b) and (c) are to be interpreted as a single neutron emission event in which the production rate varies in a complex manner; indeed, these cases are in fact degenerate with respect to the FWHM values calculated for the two peaks. The point at which the two peaks can reasonably be categorised as 'clearly differentiated' is shown in Panel (e), in which there is no overlap between the FWHM boundary times of the peaks.

From the perspective of the confinement time calculation, it becomes evident that not all of the FWHM values calculated for all identified peaks should necessarily be included for the summation in Eq. (5). In particular, any *peak-in-a-peak* scenarios (see Panels (c) and (d) of Fig. 1) lead to overestimating the total confinement time; potentially many similar FWHM durations can be obtained from an undifferentiated, multi-peak structure, when only a single value is required. Thus, in general the FWHM duration of a single neutron emission event must be defined in such a way as to remove and/or merge the contributions from all fully/partially overlapping peaks contained within it.

In order to handle cases with an arbitrary degree of complexity, we have developed a recursive algorithm which merges or removes the boundary times of partially/entirely overlapping peaks, resulting in a robust characterisation of the total confinement time. Having identified all the peaks in all sub-regions, then for each sub-region we successively compare each peak to the previous one within the list of peaks belonging to it. Two tests are considered for each comparison:

1. The early boundary time of a given peak is less than the late boundary time of the previous peak, i.e. $t^j_{-1/2}<t^{j-1}_{+1/2}$
2. The late boundary time of a given peak is less than the late boundary time of the previous peak, i.e. $t^j_{+1/2}<t^{j-1}_{+1/2}$

If either of the above tests are met individually this indicates that the peaks partially overlap. In this case a new peak is created with $t_{-1/2}=\min(t^{j-1}_{-1/2},t^j_{-1/2})$ and $t_{+1/2}=\max(t^{j-1}_{+1/2},t^j_{+1/2})$, and the original two peaks are removed from the list. If both conditions are met, the second peak is fully encompassed by the first, and is removed from the list. If neither condition is met the

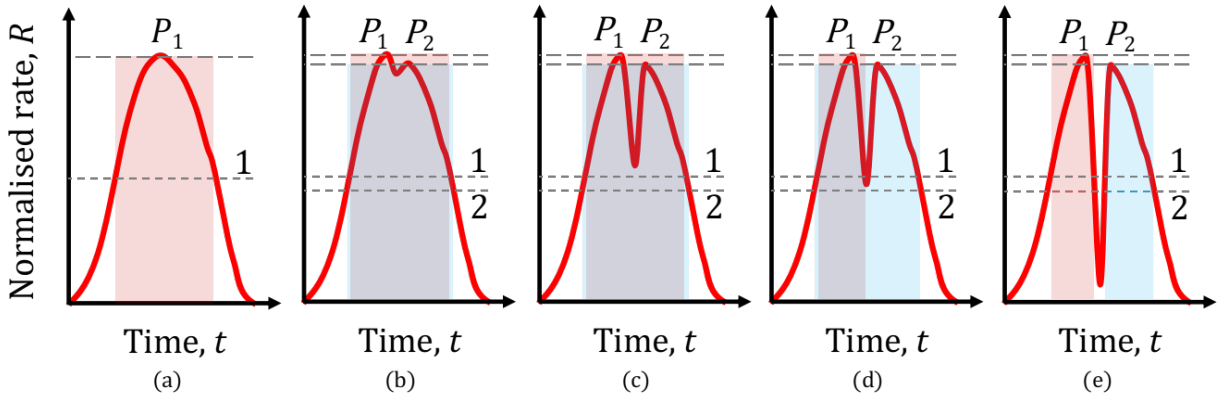

Figure 2. **Characterisation of different peak structures**: The development of an unambiguous single peak structure into a pair of distinct, clearly differentiated peaks is shown. In each panel, the upper dashed lines represent the amplitudes of the peaks and the dashed lines roughly half-way up the y-axis denote their half-amplitudes. Note that the amplitudes of two developing peaks are held constant across Panels (b-e), with only the amplitude of the inter-peak valley decreasing. (a): a single peak (P1) is present, and is characterised by a single FWHM period (maroon shaded region). (b): a second peak (P2) of similar amplitude to 1 is introduced, and the valley between them is very shallow. Applying the FWHM calculation to both peaks results in FWHM regions for both peaks that contain each other, with $\text{FWHM}_1 < \text{FWHM}_2$. (c): The amplitude of the inter-peak valley is increased, but, crucially, is greater than the half-amplitudes of either peak; this is a fully degenerate situation to Panel (b). (d): The amplitude of the inter-peak valley is now greater than the half-amplitude of P2 but remains less than the half-amplitude of P1. In this case the FWHM of P1 does not contain P2, but remains fully encompassed within FWHM_2. (e): The amplitude of the inter-peak valley is less than the half-amplitudes of both P1 and P2. Both peaks are now clearly differentiated, as there is no overlap of the boundary times of their FWHM regions.

algorithm moves on to the next peak comparison for the sub-region. If a change is made to the list of peaks, the algorithm is re-run for the modified list of peaks; this allows the method to work for cases where there are multiple peak overlaps within a single sub-region. After this algorithm has been run the result is a list of pairs of boundary times that can be unambiguously associated with all the distinct neutron emission events in a particular sub-region.

Considering the example shown in Panel (d) of Fig. 1, the algorithm successfully identifies and removes both boundary times (early and late) associated with the fourth peak in the list for sub-region 1 (blue curve) prior to refinement. The result is three distinct neutron emission events in sub-region 1, the third of which contains two undifferentiated peaks. The boundary times of all surviving neutron emission events can be seen as the shaded regions in Panel (a) of Fig. 4.

5. *Convergence of total confinement time as a function of f*

The final point that requires discussion with respect to the confinement time is its dependence on the free parameter f introduced in Eq. (9) for defining the different sub-regions. Considering again the test simulation shown in Fig. 1, it is clear that the total confinement time changes substantially as f is increased from 0.5 to 0.99. It should be expected that as $f \to 1$ then the confinement time should asymptotically approach the total run time of the simulation. For simulations where the total

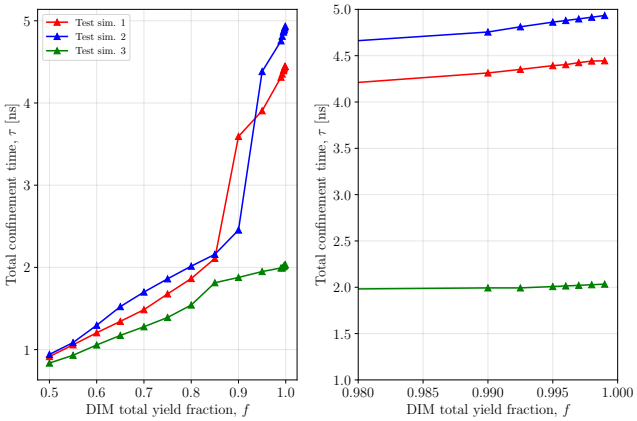

Figure 3. **Dependence of the calculated total confinement time on the DIM total yield fraction** f: Three test simulations are considered, with test simulation 1 being that used in Fig. 1, and test simulations 2 and 3 being variants with modest changes in set-up configuration. The behaviour of the data in the highly zoomed-in range $0.9 \leq f < 1$ is shown in the right-hand panel.

yield is heavily concentrated into a number of emission events, one would expect that the total confinement time should convergence to a value consistent with the duration of the established neutron emission events. This is not always guaranteed, however, since if f approaches unity too closely then the threshold value R_0 used in determining the sub-regions of interest becomes so close

to zero that contributions from regions with negligibly small yields end up being added to the total confinement time. To combat this pathology we only include contributions from neutron emission events whose fractional yield is greater than 1% of the sum over all events. The result is shown in Fig. 3, wherein it is clear that stable converged results for the total confinement time are approached as f tends to unity. We find in general that the confinement time calculated using $f = 0.99$ is always a reasonable estimate. Given the approximate nature of the definition itself we choose this as the default value for all calculations.

B. Average fuel conditions

Now that the confinement time has been defined it remains to describe how the characteristic values for the thermodynamic state of the fuel ions are treated. Given that the confinement time is the sum over multiple neutron emission events, it seems appropriate to consider an average value of the single temperature and number density values which characterise each event. The weighting of the contribution of each event should of course consider its importance to the total target performance.

Although a number of different methods for approximating the weights may be envisioned, we have chosen to use the neutron yields due to the events, such that the values used in computing the Lawson number are:

$$\langle X \rangle_{\mathrm{f}} = \frac{\sum_{\mathrm{events}} Y_{\mathrm{event}} \langle X \rangle_{\mathrm{event}}}{\sum_{\mathrm{events}} Y_{\mathrm{event}}} \,. \tag{16}$$

Here, the symbol X stands for either T_i or n_i; these are referred to as the 'fusion performance average' (FPA) values of the temperature and number density. The yield associated with a particular neutron emission event is defined as

$$Y_{\mathrm{event}} = \int_{t_{-1/2}}^{t_{+1/2}} \mathrm{d}t \, \frac{\partial Y(t)}{\partial t} \,. \tag{17}$$

Weighting by the fractional event yields in constructing the FPA values ensures that contributions due to transient simulation artefacts do not overly distort the estimate of the overall fusion performance. The final step in the methodology is to define the characteristic values for each event, $\langle T_i \rangle_{\mathrm{event}}$ and $\langle n_i \rangle_{\mathrm{event}}$, such that the Lawson number

$$L \, [\mathrm{keV\,s/m^3}] \approx \langle n_i \rangle_{\mathrm{f}} \, [1/\mathrm{m^3}] \times \langle T_i \rangle_{\mathrm{f}} \, [\mathrm{keV}] \times \tau \, [\mathrm{s}] \,, \tag{18}$$

can be constructed for a given simulation.

1. Fuel ion temperature

With respect to the ion temperature, the accepted experimental procedure involves measuring the broadening of the neutron spectrum emitted by a fusion target, which may be correlated with both the thermal and bulk hydrodynamic motion of the fuel ions [8, 9].

Without considering complexities such as synthetic diagnostics modelling, it suffices to use the burn-weighted average (BWA) of the ion temperature [10, 11]

$$\begin{aligned} \langle T_i \rangle_{\mathrm{b}}(t) &= \left(\int \mathrm{d}V \frac{\partial^2 Y(\mathbf{r},t)}{\partial V \partial t} \right)^{-1} \int \mathrm{d}V \frac{\partial^2 Y(\mathbf{r},t)}{\partial V \partial t} \, T_i(\mathbf{r},t) \\ &= \left(\frac{\partial Y(t)}{\partial t} \right)^{-1} \int \mathrm{d}V \frac{\partial^2 Y(\mathbf{r},t)}{\partial V \partial t} \, T_i(\mathbf{r},t) \,, \end{aligned} \tag{19}$$

as a reasonable surrogate for the temperature history of the fuel associated with periods of neutron emission. Indeed, the utility of the BWA ion temperature as a reliable indicator for the overall fusion performance of FLF targets has been studied through multivariate sensitivity studies [12]. In Eq. (19), the prefactor features the rate of total neutron production (accounting for all fusion reaction channels) and the weighting kernel in the integral is its derivative with respect to volume. Ignoring depletion of the fuel ion populations in the thermonuclear reactions it is reasonable to write $\partial^2 Y / \partial V \partial t \sim \frac{1}{2} n_{\mathrm{D}}^2 \langle \sigma v \rangle_{\mathrm{d(D,^3He)n}}$ for fuels whose only reactive element is deuterium and $\partial^2 Y / \partial V \partial t \sim n_{\mathrm{D}} n_{\mathrm{T}} \langle \sigma v \rangle_{\mathrm{d(T,\alpha)n}}$ if a deuterium-tritium mixture is present. The reactivities in the foregoing expressions may be computed in FLF's codes using a number of different approximations, with the most common being that of Bosch and Hale [13]. Note that in the most general case of a strongly burning fuel, featuring significant fusion product deposition and evolution of the partial densities of fuel ions, $\partial^2 Y / \partial V \partial t$ must be evaluated with a suitably detailed set of rate equations [8].

The average value of the BWA ion temperature over the duration of each event is straightforwardly

$$\langle T_i \rangle_{\mathrm{event}} = \frac{1}{\tau_{\mathrm{event}}} \int_{t_{-1/2}}^{t_{+1/2}} \mathrm{d}t \, \langle T_i \rangle_{\mathrm{b}}(t) \,. \tag{20}$$

This definition underlines the importance of the characterisation of the neutron emission events, as described in the discussion of the confinement time.

2. Fuel ion number density

Although the standard probes produced by FLF's codes do not track the BWA of the ion number density, the BWA of the total mass density of the fuel, $\langle \rho \rangle_{\mathrm{b}}(t)$, is tracked. The latter is calculated with an equivalent expression to Eq. (19) in which the ion temperature is exchanged for the mass density. For targets featuring 'simple' fusion fuels, such as mixtures of deuterium-tritium, the necessary conversion to the ion number density is trivial; one simply takes the ratio

$$\langle n_i \rangle_{\mathrm{b}}(t) = \frac{\langle \rho \rangle_{\mathrm{b}}(t)}{m_i} \,. \tag{21}$$

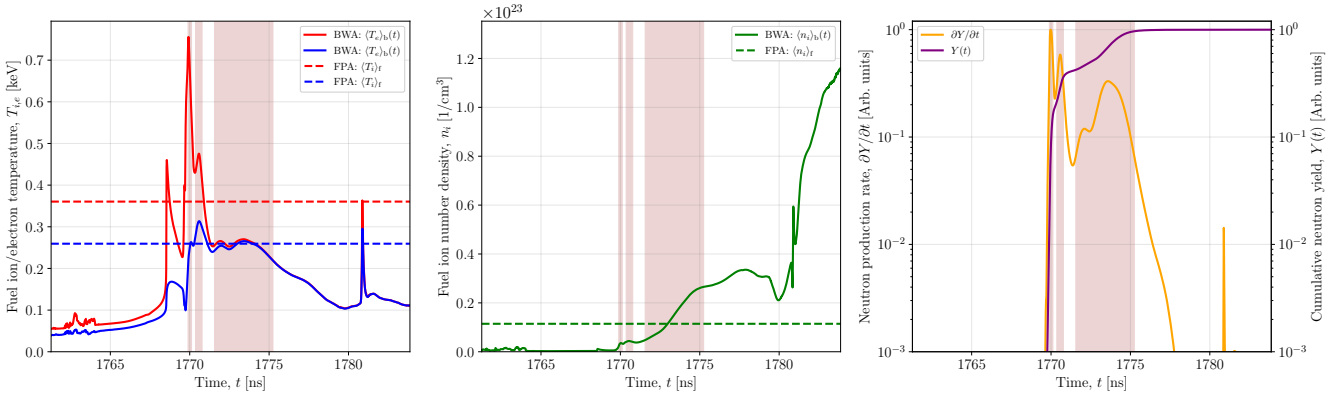

(a) Test simulation 1: as featured in Fig. 1.

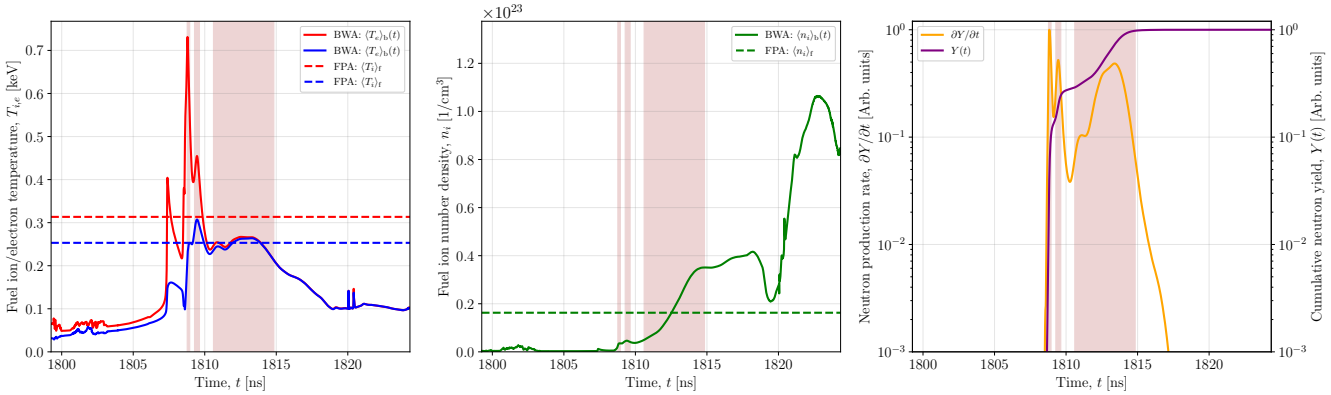

(b) Test simulation 2: a minor variation on test simulation 1, not showing the numerical artefact at late time.

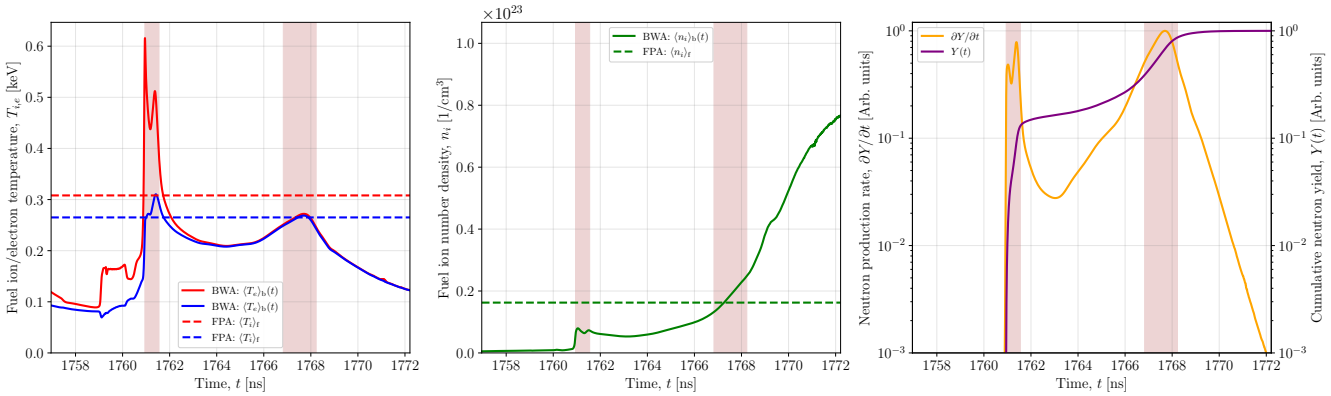

(c) Test simulation 3: this case shows two distinct neutron emission events, separated by ~ 6 ns.

Figure 4. **BWA histories, FPA values and neutron production for different test simulations:** In each case the BWA/FPA ion and electron temperatures are shown in Panel (a), the fuel ion number density in Panel (b), and the normalised total neutron production rate and cumulative neutron yield in Panel (c). The semi-transparent brown-shaded regions delineate the distinct neutron emission events computed according to the process described in Sec. II A.

Here, $m_i = \sum_a x_a m_a$ is the abundance-weighted mean ion mass, $x_a = n_a / n_i^{\text{tot}}$ is the abundance (density fraction) of a particular species, and $n_i^{\text{tot}} = \sum_a n_a$ is the total ion number density. The subscript a denotes the elemental constituents of the material. If the reactive fuel ions are mixed with a number of inert species, then Eq. (21) must be modified. The total mass density of the fuel material (assumed to be uniform in composition in space) is the sum over all the sets of all reactive ($\mathbb{R}$) and

inert ($\mathbb{I}$) ion species

$$\rho(t) = n_i^{\mathrm{tot}}(t) \sum_{a\in\mathbb{R},\mathbb{I}} x_a m_a \,, \tag{22}$$

so that the number density of a particular species in the fuel material is

$$n_a(t) = \frac{x_a \rho(t)}{\sum_{a\in\mathbb{R},\mathbb{I}} x_a m_a} \,. \tag{23}$$

Since the only time-dependent component of Eq. (23) appears in the numerator, then one may simply define an effective mass for the reactive ions for a particular simulation, such that

$$\langle n_i \rangle_{\mathrm{b}}(t) = \frac{\langle \rho \rangle_{\mathrm{b}}(t)}{m_i^{\mathrm{react}}} \,, \quad m_i^{\mathrm{react}} = \frac{\sum_{a\in\mathbb{R},\mathbb{I}} x_a m_a}{\sum_{a\in\mathbb{R}} x_a} \,. \tag{24}$$

In Fig. 4, the BWA histories for the temperature and number density of the fuel ions (and electrons) extracted from the example simulation used in Fig. 1 are shown, along with two variations. The corresponding values of the FPA values for each quantity are represented by the colour-coded, dashed horizontal lines. In each case the total neutron production rate and cumulative neutron yield (normalised to their peak values) are respectively plotted in the third panel on the left/right-hand y-axes, using a logarithmic scale. The semi-transparent brown-shaded regions on each panel denote the FWHM time boundaries of the distinct neutron emission events.

Of particular interest is the third test simulation shown in Panel (c) of Fig. 4. In this case there are two distinct neutron emission events separated by ~ 6 ns. Without the process of peak identification outline in this section, this time could have contributed towards the total confinement time, increasing the triple product value. It might be arguable that this is reasonable given that both emission events come from one holistic process, but we have chosen to be conservative. This example clearly shows the utility of our generalisations.

III. RESULTS

With the methodology defined we may now estimate the Lawson number (and related quantities) of different FLF targets and compare to the results compiled from Wurzel's fusion energy base website. In Fig. 5, the data are presented in the form of Fig. (25) from Ref. [3], showing the Lawson number versus the characteristic fuel ion temperature for the different fusion schemes considered. The data point labelled 'fusion measured' successfully measured a neutron yield [1] in close agreement with pre-shot predictions; i.e., the yield over clean (YOC factor) is of order unity. Therefore, the associated Lawson number, which is based purely the on simulation data presented in Ref. [2], may reasonably be taken to be indicative of the 'true' value that would be measured experimentally.

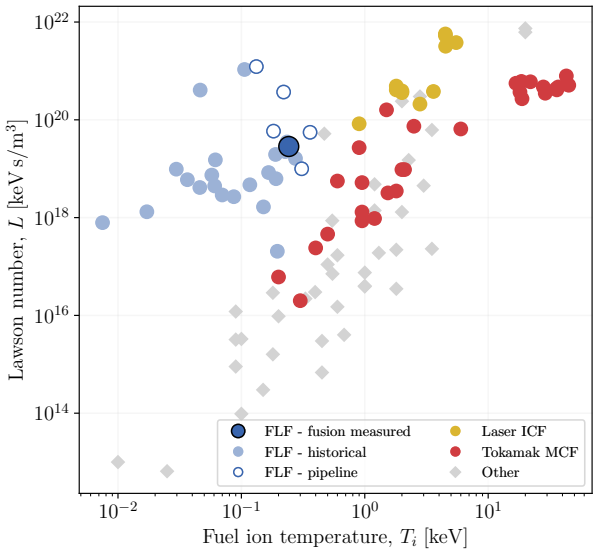

Figure 5. **Lawson number versus characteristic fuel ion temperature**: Results from Tokamak MCF (red circles), laser-driven ICF (gold circles) and other schemes (grey diamonds) are plotted along with FLF's historical (pale blue circles), current (dark blue circle with black edge) and pipeline/-future (dark blue circles with white-faces) data. The single point denoting FLF's current result with a neutron yield is discussed in Ref. [1].

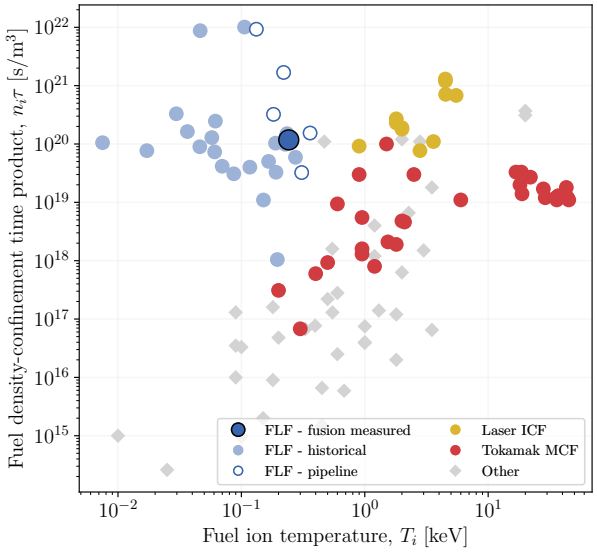

Figure 6. **Density-confinement time product versus characteristic fuel ion temperature**: Same as in Fig. 5, but plotting the fuel ion temperature against the density-confinement time product.

It is interesting to note the locus followed through the triple product parameter space as FLF's designs have improved. Most visible in Fig. 6, the trajectory is un-

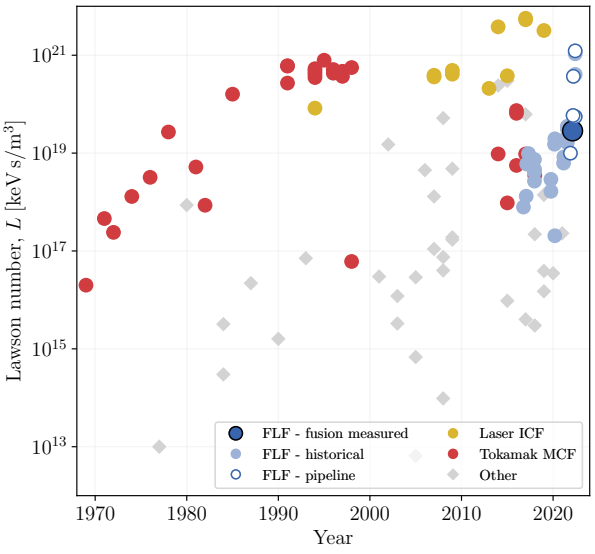

Figure 7. **Lawson number versus progression over time (year)**: Same as in Fig. 5, but plotting the year associated with the data points against the Lawson number. The extremely rapid rate of progression at FLF is clearly demonstrated in the sharp increase in estimated Lawson number since 2020, following the regular deployment of cutting-edge machine learning and optimisation methods in target design, as well as a vastly improved manufacturing capability.

usual because it starts from a point of very high values of $n_i\tau$. Over time the temperature has increased but the $n_i\tau$ value has remained within a certain window. There are three designs with a much higher value of $n_i\tau$ which stand out; these three points all come from one family of target designs and are a separate group from the other FLF designs. The value of $n_i\tau$ for these designs is higher than any other point in the fusion energy base dataset. It is important to note that despite this high value, the temperature is still low; these are not ignition designs. More generally, the neutron yield has a different dependence on the three underlying values to the triple product itself. This can readily be understood since the triple product is linear with temperature, whereas for the dependence of the fusion reactivity on temperature is generally far stronger [13]. This further explains why FLF has been climbing a substantial slope in getting to first demonstration of fusion, even though the triple product numbers may give a different impression. Finally, Fig. 7 shows triple product progress over time, showing that FLF has been making sustained, rapid progress over the last several years.

Given that the methodology presented in this work is completely general with respect to target geometry and the detail of the neutron production history, we suggest that it may serve as a useful future standard when calculating ICF triple product numbers for cross-device comparison in the global fusion community. Whilst it is unlikely that all the details and idiosyncrasies of a particular system can be encapsulated in the detail that a bespoke, device-centric analysis could, the utility of this work is that it defines a universal system which can be applied to simulations of arbitrary systems, both historical and contemporary.

IV. CONCLUSIONS

In this letter a robust methodology for calculating the Lawson number (fusion triple product) based solely on simple simulation output has been presented. The approach is generalised to target designs with complex, e.g., non-spherical, geometries in which the total neutron yield is produced in arbitrarily many 'emission events'. The total confinement time used to compute the Lawson number accounts for all distinct emission events and in the limit of a single pulse of neutrons, as encountered in conventional hot spot ICF designs, reduces to (other than a constant of proportionality) the accepted definition discussed by Chistopherson, Betti and Lindl [6]. In deciding which peaks in the total neutron production rate should be considered distinct, cases where peaks partially or fully overlap are accounted for.

For the average conditions in the fusion fuel; the temperature and number density of fuel ions, a weighted average over all emission events is used. The contribution to the temperature/number density from each emission event is given by the time-averaged value of the (time-dependent) burn-weighted average over its FWHM duration. This definition was inspired by simulation metrics discussed across ICF research: see, e.g., Weber et al. [11] and has also been used effectively for convergence studies at FLF [10]. Thus, the reaction rate of the fusion fuel within the reacting volume is fundamental in estimating the state of the system over its evolution.

Applying the methodology to simulations of historical, contemporary and future pipeline FLF targets, we have shown that the trajectory taken through the Lawson number - temperature space is unique in comparison to the data taken from `www.fusionenergybase.com`. In particular, our recent result in which fusion was successfully measured occurs at a point on the plane where a roughy ten-fold increase in fuel ion temperature would lead to results in the same territory occupied by major national laboratories, such the Omega and NIF lasers. We therefore expect the framework presented here to be useful in guiding further optimisation and refinement of target designs.

[1] G. C. Burdiak, J. W. Skidmore, J. R. Allison, R. L. Barker, H. W. Doyle, E. M. Escauriza, N.-P. L. Niasse, Z. Pešić, T. J. Ringrose, and N. A. Hawker. 0485: Vali-

date Production of Neutrons From Gas Gun-Driven Targets. Technical report, First Light Fusion Ltd., 2022.

[2] J. D. Pecover, J. W. Skidmore, N.-P. L. Niasse, M. R. Betney, D. A. Chapman, and N. A. Hawker. Simulation of the Nevarro Target. Technical report, First Light Fusion Ltd., 2022.

[3] S. E. Wurzel and S. C. Hsu. Progress toward fusion energy break-even and gain as measured against the Lawson criterion. *arXiv*, 2105.10954v4, 2022.

[4] J. D. Lawson. Some criteria for a power producing thermonuclear reactor. *Proceedings of the Physical Society. Section B*, 70:6, 1957.

[5] R. Betti, P. Y. Chang, B. K. Spears, K. S. Anderson, J. Edwards, M. Fetenejad, J. D. Lindl, R. L. McCrory, R. Nora, and D. Shvarts. Thermonuclear ignition in inertial confinement fusion and comparison with magnetic confinement. *Physics of Plasmas*, 17:058102, 2010.

[6] A. R. Chistopherson, R. Betti, and J. D. Lindl. Thermonuclear ignition and the onset of propagating burn in inertial fusion implosions. *Physical Review E*, 99:021201(R), 2019.

[7] A. Savitzky and M. J. E. Golay. Smoothing and differentiation of data by simplified least squares procedures. *Analytical Chemistry*, 36:1627, 1964.

[8] B. Appelbe and J. Chittenden. The production spectrum in fusion plasmas. *Plasma Physics and Controlled Fusion*, 53:045002, 2011.

[9] T. J. Murphy. The effect of turbulent kinetic energy on inferred ion temperature from neutron spectra. *Physics of Plasmas*, 21:072701, 2014.

[10] D. A. Chapman, J. D. Pecover, N. Chaturvedi, N. Niasse, M. P. Read, D. H. Vassilev, J. P. Chittenden, N. Hawker, and N. Joiner. A preliminary assessment of the sensitivity of uniaxially driven fusion targets to flux-limited thermal conduction modeling. *Physics of Plasmas*, 28:072702, 2021.

[11] C. R. Weber, D. S. Clark, A. W. Cook, D. C. Eder, S. W. Haan, B. A. Hammel, D. E. Hinkel, O. S. Jones, M. M. Marinak, J. L. Milovich, P. K. Patel, H. F. Robey, J. D. Salmonson, S. M. Sepke, and C. A. Thomas. Three-dimensional hydrodynamics of the deceleration stage in inertial confinement fusion. *Physics of Plasmas*, 22:032702, 2015.

[12] D. A. Chapman, D. H. Vassilev, M. P. Read, N. Chaturvedi, A. R. Fraser, R. Bordas (R), N. Joiner (R), and N. A. Hawker (R). 0405: Undertake a Comprehensive Sensitivity Study of the Kaliski Target (FITZROY-TYNE). Technical report, First Light Fusion, 2020.

[13] H.-S. Bosch and G. M. Hale. Improved formulas for fusion cross-sections and thermal reactivities. *Nuclear Fusion*, 32(4):611, 1992.